Relaxation of exciton and photoinduced dimerization in crystalline C_{60}

Masato Suzuki and Takeshi Iida
Department of Physics, Graduate School of Science, Osaka City University, Sumiyosi-ku, Osaka 558, Japan

Keiichiro Nasu
Institute of Materials Structure Science, The Graduate University for Advanced Studies, 1-1, Oho, Tukuba, Ibaraki 305, Japan

(Received 4 June 1999; revised manuscript received 17 September 1999)

We numerically investigate the lattice relaxation of photogenerated exciton in crystalline C_{60} so as to clarify the mechanism of the photoinduced dimerization processes in this material. In our theory, we deal with the π electrons together with the interatomic effective potentials. Calculations are mainly based on the mean-field theory for interelectron interactions but are also reinforced by taking the electron-hole correlation into account, so that we can obtain the exciton effect. Using a cluster model, we calculate the adiabatic potential energy surfaces of the excitons relevant to the photoinduced dimerization processes occurring in a face-centered-cubic crystal of C_{60}. The potential surfaces of the Frenkel excitons turned out to be quite uneven with several energy minimum points during the structural changes from the Franck-Condon state to the dimerized state. This leads to the conclusion that various structural defects exist at low temperatures even in the single crystal, as an intrinsic property of this molecular crystal with a complicated intermolecular interaction. From the analysis of the potential surfaces of the charge-transfer (CT) excitons, it is confirmed that the CT exciton relaxes down to its self-trapped state, wherein the adjacent two molecules get close together. This implies that the CT between adjacent two molecules is one of mechanisms that triggers the photodimerization or the photopolymerization. The oscillator strength distributions are also calculated for various intermediate structures along the lattice relaxation path. As the dimerization reaction proceeds, the oscillator strength grows in the energy region below the fundamental absorption edge, and the lowest-energy peak, originally at about 1.9 eV, finally shifts down to about 1.7 eV in the final dimerized structure. These results clarify the electronic origins of the luminescence observed in the C_{60} single crystal. Moreover, the origins of the photoinduced absorption spectra observed by Bazhenov, Gorbunov, and Volkodav are elucidated by characteristics of the adiabatic potential energy surfaces obtained here.

I. INTRODUCTION

Since the discovery of C_{60} by Kroto *et al.*,[1] the problems related to the structures and/or the functionality of fullerene compounds have been studied very extensively from both theoretical and experimental points of view.[2] It is now well established that the C_{60} molecule consists of the 60 equivalently bonded carbon atoms that construct the soccer-ball cage structure. In this cage, each carbon is linked with three carbons through four bonds; three σ bonds and one π bond, which is located at the fusion between hexagonal rings. It has been confirmed that the intercarbon distances of single and double bonds are 1.45 and 1.40 Å, respectively.[3] In crystalline C_{60}, the molecules are bound together by weak van der Waals forces and are positioned in a close-packed array of a face-centered-cubic (fcc) lattice, with a lattice constant of 14.2 Å. As is well known, the C_{60} crystal undergoes a structural phase transition from the fcc to the simple cubic at the temperature $T_c = 260\,\mathrm{K}$.[4] Above T_c, the molecules rotate almost randomly around their lattice positions. The molecular rotation becomes restricted below T_c and it is finally frozen at 90 K. In this frozen configuration, the three fold axes of molecules orient the different (111) directions in a unit cell, wherein the pentagonal ring in one molecule faces the double bonds of the neighboring molecules.[5]

The polymerization has been reported to occur above T_c by optical excitations with visible or uv light,[6] and this phenomenon is induced by the high pressure and high temperature as well.[7] In this polymer phase, it was proposed that the adjacent molecules are covalently linked by a four-membered ring joining the two molecular cages. Thus, the intermolecular bond changes from the van der Waals type to covalent as a consequence of the optical excitation. A photochemical $[2+2]$ cycloaddition reaction was also proposed as a mechanism of the photoinduced dimerization in crystalline C_{60}. However, the detailed mechanisms of the photoinduced formation of intermolecular covalent bonds have still been left unsolved.

In order to see a role of the optical excitation in the dimerization process, let us briefly mention the nature of excitons and their lattice relaxations in molecular crystals such as C_{60}. In general, the photoexcitation in an insulator creates an electron and a hole, and they attract each other through the Coulombic interaction so as to make an exciton. After the exciton is thus generated, it interacts with the lattice vibrations (or phonons) through the electron-phonon coupling, and this interaction brings about various lattice relaxation processes.[8,9] When we consider the interaction between excitons and phonons in molecular crystals, it is useful to classify the excitons into three types; free, Frenkel, and charge-transfer (CT) excitons, according to the distribution patterns of the electron-hole pair. In the free or bulk exciton, the electron-hole pair can travel almost freely through the whole crystal. Hence, the coupling between free excitons and mo-

lecular vibrations is expected to be rather weak. The Frenkel exciton is basically an intramolecular excited state, and its motion is mainly restricted in one molecule, while only rarely does it hop to other molecules through a weak intermolecular interaction. Therefore, the Frenkel exciton will strongly interact with intramolecular rather than intermolecular vibrations (lattice phonons). On the other hand, in the case of the CT exciton, an electron and a hole are divided into two adjacent molecules, and they interact through the Coulombic force so as to make the intermolecular excitonic state. This means that the interaction between the CT exciton and the lattice phonons is strong compared with the case of Frenkel exciton, and this interaction brings about the large intermolecular lattice relaxations of the CT excitons. Hereafter, we will be concerned with photoinduced dimerization, and in this case the two adjacent molecules need to be close to each other at the initial stage of this process. Therefore, the CT followed by the lattice relaxation will be the key mechanism of photodimerization.

In the present paper, we investigate the adiabatic natures of the lattice relaxation of the photogenerated exciton in crystalline C_{60}, so as to clarify the mechanisms of the photoinduced-dimerization process in this crystal. Moreover, we calculate the oscillator-strength distributions for various intermediate structures along the dimerization process, in order to clarify the recent spectroscopic studies on the structural changes induced by light. Finally, we discuss the characteristics of the photoinduced structural phase transition occurring in such molecular crystals.

II. THEORETICAL METHODS

A. Model Hamiltonian

In order to clarify the mechanism of the photodimerization processes in crystalline C_{60}, we investigate a many-π-electron system described by the following model Hamiltonian ($\equiv H$), wherein the elastic energies between carbons are taken into account by effective potentials. H is given as ($\hbar \equiv 1$)

$$H = H_{\text{intra}} + H_{\text{inter}}, \tag{2.1}$$

$$H_{\text{intra}} = \sum_{l,\sigma,i} \varepsilon_{li} a^{\dagger}_{li,\sigma} a_{li,\sigma} + \sum_{l,\sigma,i>j} (-T^{ll}_{ij} a^{\dagger}_{li,\sigma} a_{lj,\sigma} + \text{H.c.}) + U \sum_{l,i} n_{li,\alpha} n_{li,\beta} + \sum_{l,\sigma,\sigma',i>j} V^{ll}_{ij} n_{li,\sigma} n_{lj,\sigma'} + \sum_{l,i>j} \omega^{ll}_{ij}, \tag{2.2}$$

$$H_{\text{inter}} = \sum_{l>l',\sigma,i,j} (-T^{ll'}_{ij} a^{\dagger}_{li,\sigma} a_{l'j,\sigma} + \text{H.c.}) + \sum_{l>l',\sigma,\sigma',i,j} V^{ll'}_{ij} n_{li,\sigma} n_{l'j,\sigma'} + \sum_{l>l',i,j} \omega^{ll'}_{ij}, \tag{2.3}$$

$$n_{li,\sigma} \equiv a^{\dagger}_{li,\sigma} a_{li,\sigma}. \tag{2.4}$$

H_{intra} denotes the Hamiltonian for the isolated molecules, and H_{inter} is the intermolecular interaction. l indicates the lth C_{60} molecule and l' is its nearest-neighbor molecule. i or j represents the carbon in each C_{60} molecule. $a^{\dagger}_{li,\sigma}$ ($a_{li,\sigma}$) is the creation (annihilation) operator of a π electron with spin σ ($\equiv \alpha, \beta$) at the ith carbon site in the lth molecule. The first term in Eq. (2.2) gives the site-diagonal part of the electron-phonon interaction, and ε_{li} is its interaction parameter. It is inversely proportional to the distance ($\equiv r^{ll'}_{ij}$) between the lith carbon and the other $l'j$th carbons, as described by the following formula with a fitting parameter κ:

$$\varepsilon_{li} = \sum_{(l',j)[\neq(l,i)]} \frac{\kappa}{r^{ll'}_{ij}}. \tag{2.5}$$

The terms with T^{ll}_{ij} or $T^{ll'}_{ij}$ in Eqs. (2.2) and (2.3) denote the resonance transfer integral of π electrons between carbon atoms, and it leads to the off-diagonal electron-phonon interaction. The dependency of $T^{ll'}_{ij}$ on $r^{ll'}_{ij}$ is assumed to be an exponential function with the fitting parameters, T_m and λ_X, as

$$T^{ll'}_{ij} = T_m \exp[\lambda_{\text{intra}} r_m - \lambda_X r^{ll'}_{ij}]. \tag{2.6}$$

Here, the subscript X denotes intra when $l = l'$ and inter when $l \neq l'$. T_m is the resonance transfer integral for the mean bond distance in the molecule [$\equiv r_m = (r_s + r_d)/2$]. U and V^{ll}_{ij}($V^{ll'}_{ij}$) denote the intrasite and intersite Coulombic repulsive energies, respectively. We use the Ohono potential for this $V^{ll'}_{ij}$ as

$$V^{ll'}_{ij} = \frac{1}{\sqrt{(1/U)^2 + (\delta_X r^{ll'}_{ij})^2}}, \tag{2.7}$$

where δ_X is the screening constant defined by $1/(r_m V_X)$. V_X is a parameter to be determined later. ω^{ll}_{ij} and $\omega^{ll'}_{ij}$ in the last terms of Eqs. (2.2) and (2.3) are the elastic energies between carbon sites and are defined as

$$\omega^{ll'}_{ij} = k_X \left[\left(\frac{r_0}{r^{ll'}_{ij}} \right)^{12} - 2 \left(\frac{r_0}{r^{ll'}_{ij}} \right)^{6} \right] + \frac{k}{r^{ll'}_{ij}}, \tag{2.8}$$

where we use the Lennard-Jones potential with fitting parameters k_X and r_0 for the short-range interaction. This potential implicitly includes the effects of σ bonding between carbons. In order to correct the Lennard-Jones potential for the long-range region, we add a $1/r^{ll'}_{ij}$-type potential with a fitting parameter k.

Thus, our Hamiltonian contains 11 unknown parameters: U, κ, T_m, λ_{intra}, λ_{inter}, V_{intra}, V_{inter}, k_{intra}, k_{inter}, r_0, and k, which are summarized in Table I. The parameter values are determined in the following section so as to reproduce well-known experiments.

Let us now explain our basic method to calculate the ground and excited states from Eq. (2.1). In the case of the ground state, we use the mean-field theory for interelectron interactions. Within this mean-field Hamiltonian ($\equiv H_{\text{HF}}$), $n_{li,\sigma}$ and $a^{\dagger}_{li,\sigma} a_{l'j,\sigma}$ are replaced by their averages so that

$$n_{li,\sigma} \Rightarrow \langle n_{li,\sigma} \rangle, \quad a^{\dagger}_{li,\sigma} a_{l'j,\sigma} \Rightarrow \langle a^{\dagger}_{li,\sigma} a_{l'j,\sigma} \rangle. \tag{2.9}$$

TABLE I. Summary of the unknown parameters contained in the model Hamiltonian.

Interaction energies	Formulas $X=\text{intra}(l=l'),\ \text{inter}(l\neq l')$	Fitting parameters	Determined values in bulk crystal
ε_{li}	$\sum_{(l',j)[\neq(l,i)]}\frac{\kappa}{r_{ij}^{ll'}}$	κ	-0.65 Å T_m
T_{ij}^{ll} or $T_{ij}^{ll'}$	$T_m\exp[\lambda_{\text{intra}}r_m-\lambda_X r_{ij}^{ll'}]$	T_m	2.98 eV
		λ_{intra}	1.00/Å
		λ_{inter}	1.89/Å
V_{ij}^{ll} or $V_{ij}^{ll'}$	$1/\sqrt{(1/U)^2+[r_{ij}^{ll'}/(r_m V_X)]^2}$	U	$1.90\,T_m$
		V_{intra}	$1.00\,T_m$
		V_{inter}	$0.31\,T_m$
ω_{ij}^{ll} or $\omega_{ij}^{ll'}$	$k_X[(r_0/r_{ij}^{ll'})^{12}-2(r_0/r_{ij}^{ll'})^6]+k/r_{ij}^{ll'}$	k_{intra}	$0.75\,T_m$
		k_{inter}	$0.025\,T_m$
		r_0	1.429 Å
		k	0.48 Å T_m

These $\langle n_{li,\sigma}\rangle$ and $\langle a_{li,\sigma}^{\dagger}a_{l'j,\sigma}\rangle$ are unknown parameters to be determined later self-consistently. By diagonalizing this H_{HF}, we can obtain energies of the ground and excited states. In order to take the electron-hole correlation into account in the excited state, we define the difference ($\equiv\Delta H$) between the true Hamiltonian and the mean-field one as

$$\Delta H=H-H_{\text{HF}} \tag{2.10}$$

and take the expectation values of ΔH within the basis of the one-electron excited states obtained from H_{HF}. This is first-order perturbation theory for the electron-hole correlation. Then, we can determine the new energies of excited states, including the exciton effects. By working this process out for various lattice configurations, we can obtain adiabatic potential energy surfaces of the excitons.

B. Parameter values in bulk crystal

Let us determine the unknown 11 parameters included in the model Hamiltonian so as to reproduce the well-known experimental results. In the C_{60} molecule, it has been confirmed by various experiments that the energy of the lowest singlet exciton is about 1.9 eV (Ref. 10) and the energy difference between lowest singlet and triplet excitons is less than 0.2 eV (Refs. 11 and 12). Moreover, the absorption spectra have been observed for the molecule and the crystal, and they have three main peaks at the energies about 3.7, 4.8, and 5.9 eV.[13–18] In addition to these peaks, in the case of the crystal, the shoulder structure appears around 2.7 eV, which has been identified as the charge-transfer-type excitation between molecules.[19] For reference, the observed absorption spectrum for a C_{60} film is given in Fig. 1(a), which is quoted by reading off the figure in Ref. 18. To reproduce the above experimental results under the bulk structure of $r_d=1.40$ Å, $r_s=1.45$ Å, and $a_0=14.2$ Å, the parameters for π electrons, T_m, U, λ_{intra}, V_{intra}, λ_{inter}, V_{inter}, and κ are determined to be 2.98 eV, $1.90T_m$, 1.00 Å^{-1}, $1.00T_m$, 1.89 Å^{-1}, $0.31T_m$, and -0.65 Å T_m, respectively. To determine these parameters, we have used a cluster of four molecules with a periodic boundary condition instead of the real infinite crystal. We also determine the parameters contained in the elastic energy terms as $r_0=1.429$ Å, $k_{\text{intra}}=0.75T_m$, $k_{\text{inter}}=0.025T_m$, and $k=0.48$ Å T_m, so that these values give the stable structure for the ground state when r_d, r_s, and a_0 take the aforementioned values.

In order to certify the reasonableness of the parameters thus determined, we show the oscillator-strength distributions for the one-electron excitation [$\equiv I(E)$] calculated by using the following equation:

$$I(E_n-E_g)=|\langle n|\hat{P}|g\rangle|^2(E_n-E_g), \tag{2.11}$$

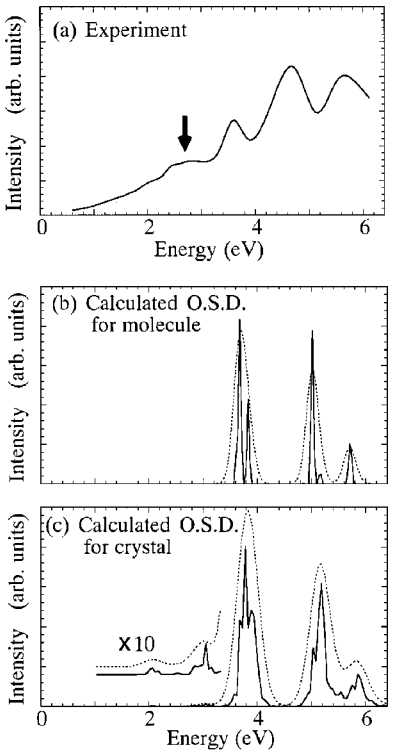

FIG. 1. (a) The observed absorption spectrum of a C_{60} film from Ref. 18, and (b) the calculated oscillator-strength distribution (OSD) for single molecule and (c) crystalline C_{60}. In (a), the absorption peak indicated by the thick arrow is observed only in the solid phase. In (b) and (c), the dotted line is the guideline of the spectral shape, which is obtained by the Gaussian fitting.

where

$$\hat{P}=i\sum_{ll',ij,\sigma}(e_{ij}^{ll'}\cdot\vec{p})\mu_{ij}^{ll'}a_{li\sigma}^{\dagger}a_{l'j\sigma}. \tag{2.12}$$

Here, $|g\rangle$ and $|n\rangle$ indicate the wave functions of the ground state and the nth one-electron excited state, respectively. E_g and E_n are their energies with the exciton effect. $\hat{P}$ denotes the polarization operator, $e_{ij}^{ll'}$ the unit vector from the li site to the $l'j$ site, $\vec{p}$ the unit vector of the polarization of light, and $\mu_{ij}^{ll'}$ the matrix element of the dipole moment. In our calculations, $\mu_{ij}^{ll'}$ is assumed to be proportional to $T_{ij}^{ll'}$. Calculated oscillator-strength distributions are shown in Figs. 1(b) and 1(c), where the former is for the single molecule and the latter is for the bulk crystal, which, as mentioned before, is approximated by the cluster of four molecules with the periodic boundary condition. In these figures, the dotted line is the guideline for the spectral shape, which is obtained by the Gaussian fitting. As seen in these figures, three peaks, which are the optically allowed, appear both in the molecule and the crystal in almost same energy regions. In the case of the crystal, the distribution peaks become broader compared with that of molecule, due to the intermolecular interaction. These features agree well with the observed absorption spectra mentioned above.[13–18]

III. ADIABATIC POTENTIAL ENERGY SURFACES FOR PHOTODIMERIZATION

A. Cluster model and lattice-distortion patterns

In order to calculate the potential energy surfaces relevant to the photoinduced dimerization in crystalline C_{60}, we use a cluster that consists of 54 C_{60} molecules arranged on the fcc lattice points. This cluster is schematically shown in Fig. 2, wherein each circle represents the C_{60} molecule, and the centered two molecules labeled by 1 and 2 are assumed to dimerize. In addition to molecules 1 and 2, the four centered molecules are denoted by the black-lacquered circles and numbered from 3 to 6. In our calculations, only these six molecules are assumed to have excited states of π electrons, and these states are solved by applying the aforementioned model Hamiltonian. The gray and open circles represent neutral C_{60}, whose π electrons are assumed to remain always in the ground state throughout our calculations. As for the center-of-mass motion of molecules, the black and gray circles are assumed to move during the dimerization, while the open circles keep their fcc lattice points. The intermolecular configurations at the ground state are chosen so that a pentagonal ring of one molecule faces a double bond of the neighboring molecules, as schematically shown by the inset in Fig. 2.

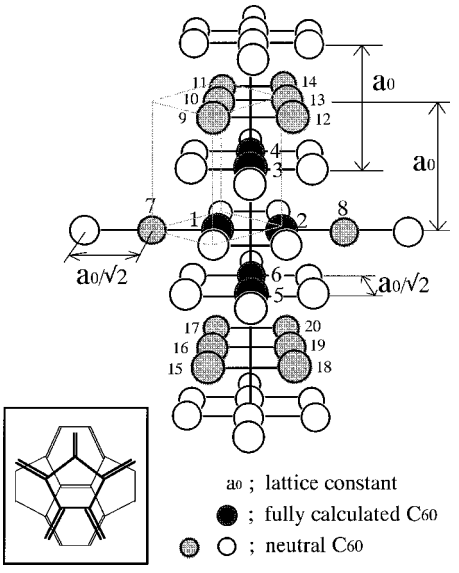

FIG. 2. Schematical structure of a cluster that consists of 54 C_{60} molecules. Each circle represents the C_{60} molecule arranged on the fcc lattice points. The two centered molecules labeled by 1 and 2 are assumed to dimerize.

Let us consider a configuration space with respect to the lattice distortion that expresses the structural changes accompanied with the $[2+2]$ cycloaddition reaction in the crystal. To open the dimerization channel, a pair of molecules will move sufficiently closer to each other, from the very beginning of the lattice relaxation. Therefore, at first, we define the displacements of the center of mass of each molecule labeled by 1 to 6, as depicted by the thick arrow in Fig. 3(a), where ΔR_t indicates the displacement of the dimerizing molecules (1 and 2) and $\Delta R_t'$ is that of the other molecules (3 to 6). These displacements are just toward the center of the cluster from each lattice point. Moreover, we take into account the displacements of the 14 molecules around these six centered molecules. They are indicated by the gray circles numbered by 7 to 20 as shown in Fig. 2. The displacements of the two molecules 7 and 8 are indicated by $\Delta R_t^{(2)}$ and those of the twelve molecules from 9 to 20 by $\Delta R_t^{(12)}$. The directions of these displacements are defined in the same way as that of ΔR_t and $\Delta R_t'$, that is, they are just toward the center of the cluster from each lattice point.

As the dimerization proceeds further, the intermolecular configurations will also be changed, and the double bonds in molecules 1 and 2 will become nearly parallel to each other. This type of motion is defined as shown in Fig. 3(b) where the thick line denotes molecule 1 and the thin line is molecule 2. As depicted by the open arrow in the inset of this figure, the two double bonds indicated by the dotted lines are assumed to be close to each other through the rotation of molecule 1 on its penetration axis, which is parallel to the dimerizing double bond of this molecule. This rotation angle from the Franck-Condon state is denoted by $\Delta\phi$, shown schematically in this figure.

As these two double bonds in the adjacent molecules come close to each other, the molecular cage itself will become distorted, so as to establish the cycloaddition reaction. In order to investigate such intramolecular structural relaxations, we take into account the displacements of the carbon atoms within molecules 1 and 2. That is, we assume that the two double bonds relevant to the $[2+2]$ cycloaddition move equally in the direction perpendicular to the molecular surface, as shown by the gray lines and arrows in Fig. 3(c). This type of displacement is designated by Δr_t.

As this $[2+2]$ cycloaddition proceeds, the dimer cage itself will also be elongated along the dimer axis as shown in Fig. 3(d), so as to release the strain energy due to this addi-

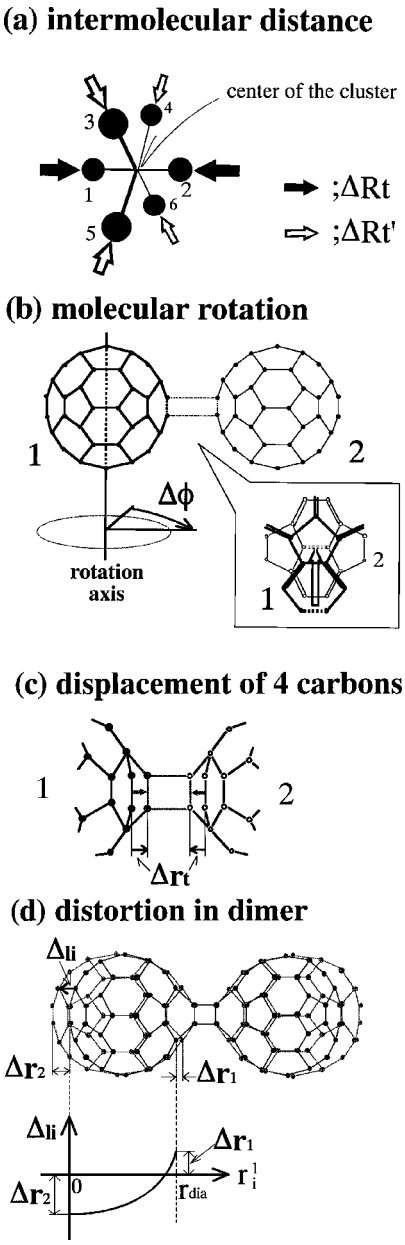

FIG. 3. The lattice-distortion patterns relevant to the photoinduced dimerization in crystalline C_{60}. (a) The displacements of the center of mass of each molecule, which is denoted by the black circle labeled by 1–6 in Fig. 2. ΔR_t indicates the displacement of the dimerizing molecules 1 and 2, and $\Delta R_t'$ is that of other molecules labeled 3–6. These displacements are just toward the center of the cluster from each lattice point. (b) The rotation of molecule 1 on its penetration axis that is parallel to the dimerizing double bond of this molecule. The thick and thin lines denote molecules 1 and 2, respectively, and the two double bonds indicated by the dotted lines are assumed to be close to each other through the rotation of molecule 1. $\Delta\phi$ denotes the rotation angle from the Franck-Condon state. (c) The displacements of the carbon atoms within molecules 1 and 2. Δr_t denotes the displacement of the two double bonds relevant to the [2+2] cycloaddition, which are assumed to equally move in the direction perpendicular to the molecular surface. (d) The intradimer lattice distortion ($\equiv\Delta_{li}$) along the dimer axis after the [2+2] cycloaddition reaction. Δr_1, Δr_2, and n are positive variational parameters. r_i^l denotes the position coordinate of lith carbon atom projected on the dimer axis. $r_{\rm dia}$ is the diameter of the C_{60} molecule.

tion. In our calculations, we will also include such an intradimer lattice relaxation by introducing the displacement ($\equiv\Delta_{li}$) of the lith carbon along the dimer axis. Then, we assume the following form for this Δ_{li}:

$$\Delta_{li}=(\Delta r_1+\Delta r_2)\left(\frac{r_i^l}{r_{\rm dia}}\right)^n-\Delta r_2, \tag{3.1}$$

where Δr_1, Δr_2, and n are positive variational parameters. In this equation, r_i^l is the position coordinate of lith carbon atom projected on the dimer axis, and it is measured from each end of the dimer. $r_{\rm dia}$ denotes the diameter of the C_{60} molecule. Of course, we assume $\Delta_{li}=0$ for the four carbon atoms that are directly concerned with the cycloaddition. Thus, Δ_{li} leads the elliptically elongated distortion along the dimer axis as seen in Fig. 3(d). In this figure, the gray lines give the schematical view of the atomic configuration after this lattice distortion.

Finally, it should be noted that these four types of distortions [(a)–(d)] shown in Fig. 3, will occur almost simultaneously. The chronological order between them is rather qualitative.

Thus, we have defined the multidimensional configuration space spanned by ΔR_t, $\Delta R_t'$, $\Delta R_t^{(2)}$, $\Delta R_t^{(12)}$, $\Delta\phi$, Δr_t, Δr_1, Δr_2, and n. These distortion parameters are summarized in Table II.

B. Structure of dimer and structural changes through dimerization

In order to determine the final structure of the dimer in crystalline C_{60}, we calculate the adiabatic potential energies of the lowest singlet exciton for various structures in the multidimensional configuration space defined above. After these calculations, we finally can get the most stable dimerized structure in the configuration space at $\Delta R_t=0.65$ Å, $\Delta R_t'=-0.20$ Å, $\Delta R_t^{(2)}=0.47$ Å, $\Delta R_t^{(12)}=-0.14$ Å, $\Delta\phi=0.375\pi$, $\Delta r_t=0.195$ Å, $\Delta r_1=0.055$ Å, $\Delta r_2=0$, and $n=4$. We schematically show the final structure of dimer in Fig. 4 by the gray lines, extracting only the two dimerized C_{60}'s from the final distorted crystal. The solid lines are a guideline to separate the intradimer lattice relaxation from the spherical atomic configuration of C_{60}.

Next, let us determine the relaxation path that starts from the Franck-Condon state in fcc and terminates at the dimerized structure obtained above. To this end, we connect these two states by an extremal path on the potential energy surface of the lowest singlet exciton in the multidimensional configuration space, so as to minimize the energy barrier between them. This path can be uniquely determined, and the structural changes along this path are depicted in Fig. 5. Each point on this path is specified by a combination of values for ΔR_t, $\Delta R_t'$, $\Delta R_t^{(2)}$, $\Delta R_t^{(12)}$, $\Delta\phi$, Δr_t, and Δr_1. Δr_2 and n are determined to be 0 and 4, respectively, through this path. However, this combination changes in a very complicated way. Hence, we introduce a simple number ($\equiv R_N$), which changes from 0 in the Franck-Condon state to 55 in the most stable dimerized state along the path. The meaning of this R_N is roughly equal to the distance from the Franck-Condon state, but it is not the exact one. It is introduced only to make the later explanations simple and easy,

TABLE II. Summary of the lattice-distortion parameters that define the multidimensional configuration space.

Symbol	Meaning	Values in most stable dimerized structure
ΔR_t	Displacement of dimerizing molecules (1 and 2)	0.65 Å
$\Delta R_t'$	Displacement of four molecules (3–6)	−0.20 Å
$\Delta R_t^{(2)}$	Displacement of two molecules (7 and 8)	0.47 Å
$\Delta R_t^{(12)}$	Displacement of twelve molecules (9–20)	−0.14 Å
$\Delta\phi$	Rotation angle of molecule 1	0.375π
Δr_t	Displacements of carbon atoms in two double bonds relevant to [2+2] cycloaddition	0.195Å
Δ_{li}	Elliptically elongated intradimer lattice distortion along dimer axis, $\Delta_{li}=(\Delta r_1+\Delta r_2)(r_i^l/r_{\rm dia})^n-\Delta r_2$	$\Delta r_1=0.055$ Å $\Delta r_2=0$ $n=4$

by reducing the path as if it were a one-dimensional one. By this R_N together with Fig. 5, we can clearly specify the structural changes in each point of the relaxation path. When $R_N=10$, for example, it can read from Fig. 5 that the corresponding structural changes in the multidimensional configuration space are $\Delta R_t\approx 0.5$ Å, $\Delta R_t'\approx -0.19$ Å, $\Delta R_t^{(2)}\approx 0.11$ Å, $\Delta R_t^{(12)}\approx -0.04$ Å, $\Delta\phi\approx 0.05\pi$, $\Delta r_t=0$, and $\Delta r_1=0$.

Dividing Fig. 5 into four regions from *A* to *D*, let us briefly see how the structure changes during the dimerization. In region *A*, the structural changes mainly come from ΔR_t and $\Delta R_t'$. As the relaxation of this region proceeds, molecules 1 and 2 come close to each other and the molecules labeled 3 to 6 depart from these two centered molecules (1 and 2), in order to avoid the repulsive interactions among them. The adiabatic potential energy surface of the lowest singlet exciton in this region is shown in Fig. 6 as a function of ΔR_t and $\Delta R_t'$. As defined above, the point with $\Delta R_t=\Delta R_t'=0$ represents the Franck-Condon state. The determined structural change is roughly expressed by the thick arrow in Fig. 6. This structural change is expected to be self-induced by the CT exciton because the potential energy surfaces of the CT excitons have a maximum gradient in the vicinity of the Franck-Condon state, which will be discussed in detail in the next section. For this region *A*, we assign R_N from 0 (in the Franck-Condon state) to 15, as shown in Fig. 5.

In region *B*, we can see that molecule 1 mainly rotates. In order to investigate the feature of rotational relaxations of the excited molecules, let us see the adiabatic potential surface of the exciton as a function of $\Delta\phi$ and ΔR_t in Fig. 7, where $\Delta R_t'$ changes together with ΔR_t through the relaxation path. In this figure, the double bonds of the adjacent molecules 1 and 2 face each other in parallel when $\Delta\phi\cong 0.375\pi$. The point near $\Delta R_t=0.8$ Å ($\Delta R_t'=-0.2$ Å) and $\Delta\phi=0.375\pi$ is regarded as a ''reaction point,'' because the double bonds in the two molecules are close enough to each other to create the four-membered ring by the cycloaddition reaction.

Judging from Fig. 7, we can see that no matter what path may be selected, the energy of the lowest singlet exciton increases as the structural changes proceed from the Franck-Condon state to the reaction point. Moreover, there are many minimum points on the potential surface, which mainly come from the difference of the molecular orientations. The ground state also has many minima at almost the same configurations of the metastable states of exciton. For this reason, these metastable configurations are regarded as structural defects with a relatively long lifetime. This will be an intrinsic property of such molecular crystals with a compli-

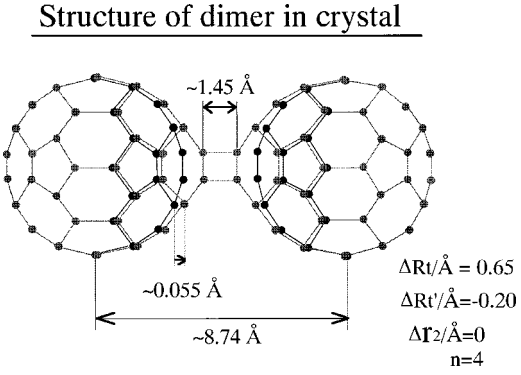

FIG. 4. Schematical view of the most stable structure of the dimer in the crystal. The gray lines denote the dimerized two C_{60}'s extracted from the final distorted crystal. The solid lines are a guideline to show clearly the intradimer lattice relaxation from the spherical atomic configuration of C_{60}.

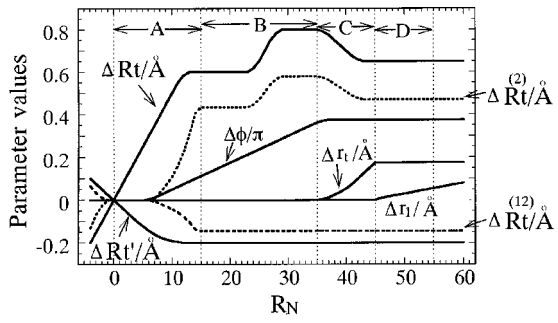

FIG. 5. The structural changes from the fcc to the dimerized structure in the multidimensional configuration space spanned by ΔR_t, $\Delta R_t'$, $\Delta R_t^{(2)}$, $\Delta R_t^{(12)}$, $\Delta\phi$, Δr_t, Δr_1, Δr_2, and *n*. R_N is a simple number to specify each point along the path, which changes from 0 for the Franck-Condon state to 55 for the dimerized structure.

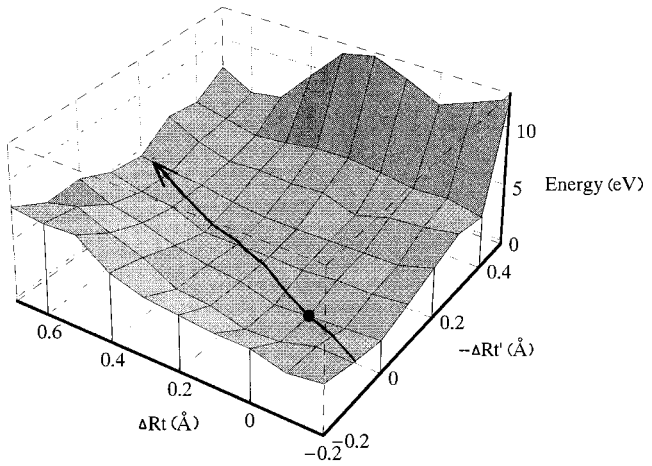

FIG. 6. The adiabatic potential energy surface of the lowest singlet exciton as a function of ΔR_t and $\Delta R_t'$.

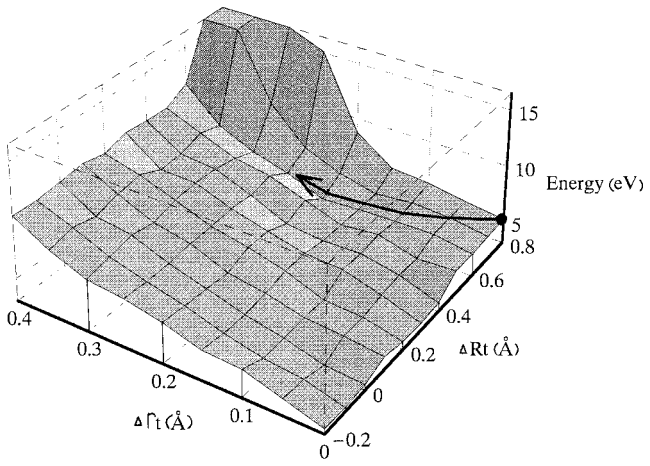

FIG. 8. The adiabatic potential energy surface of the lowest singlet exciton as a function of Δr_t and ΔR_t. $\Delta R_t'$ changes together with ΔR_t through the relaxation path determined in Fig. 6, and $\Delta\phi$ is fixed to be 0.375π.

cated intermolecular interaction. If the exciton is created at or below T_C, the molecular rotation is almost frozen, and therefore the relaxation of the lowest singlet exciton will be stopped by the energy barriers on the way and terminates up to these defects. This makes the probability to reach the aforementioned reaction point very low. In contrast, the probability will be strongly enhanced when the exciton is created by a high-energy photon under the condition of the free rotation above T_C. Thus, the relaxation of the exciton in this stage is strongly affected by the excitation energy and/or the temperature. From these features, we can find the path of the structural change from the Franck-Condon state to the reaction point as schematically shown in Fig. 7. In this path, we have assumed that the molecule begins to rotate after the two molecules approach to a certain distance, and then the double bonds become parallel through the typical energy minima. For this region *B*, we assign R_N from 15 to 35, as shown in Fig. 5.

Regions *C* and *D* are concerned mainly with the structural changes after the dimerization is almost completed. Especially, the structural changes in region *C* mainly come from ΔR_t and Δr_t. We show the adiabatic energy surface of the exciton on the ΔR_t-Δr_t plane in Fig. 8, while $\Delta R_t'$ changes through the path as depicted in Fig. 6 and $\Delta\phi$ is fixed as 0.375π. From this figure, it can be seen that the energy minimum point appears in the vicinity of $\Delta R_t = 0.65$ Å ($\Delta R_t' = -0.2$ Å) and $\Delta r_t = 0.195$ Å. Therefore, the relaxation path from the reaction point of $\Delta R_t = 0.8$ Å to the minimum on this potential is indicated in Fig. 8 by a thick arrow. As the reaction proceeds through this path, ΔR_t decreases and at the same time Δr_t increases, that is, the two molecules slightly separate from each other with almost no change in the structure of the four-membered ring. We assign $R_N = 35-45$, for this region *C*.

Finally, the lattice relaxation described in Fig. 3(d) occurs in region *D*. The potential energy surface of the exciton is depicted in Fig. 9 as a function of Δr_1 and n with the fixed values of $\Delta R_t = 0.65$ Å, $\Delta R_t' = 0.2$ Å, $\Delta\phi = 0.375\pi$, and $\Delta r_t = 0.195$ Å. Δr_2 has been chosen to be zero, because we cannot find any energy minimum with respect to this parameter. As shown in this figure, we get the most stable dimerized structure at $\Delta r_1 = 0.055$ Å and $n = 4$. The relaxation

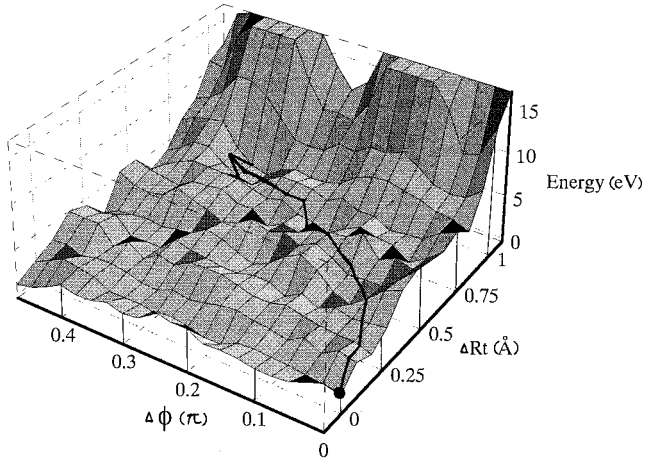

FIG. 7. The adiabatic potential energy surfaces of the lowest singlet exciton as a function of $\Delta\phi$ and ΔR_t. $\Delta R_t'$ changes together with ΔR_t through the relaxation path determined in Fig. 6.

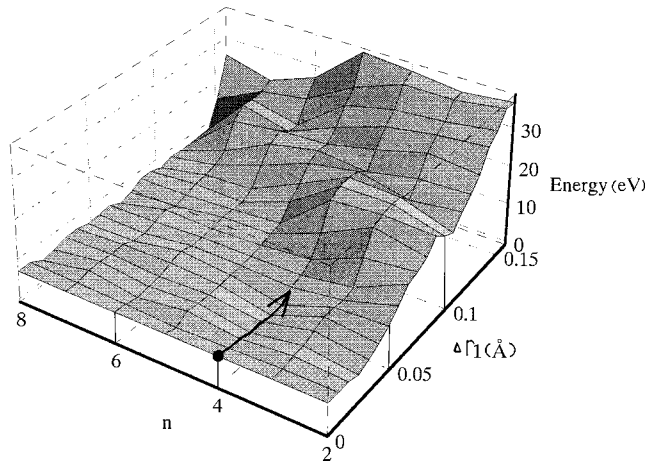

FIG. 9. The adiabatic potential energy surface of the lowest singlet exciton as a function of Δr_1 and n with the fixed values of $\Delta R_t = 0.65$ Å, $\Delta R_t' = 0.2$ Å, $\Delta\phi = 0.375\pi$, and $\Delta r_t = 0.195$ Å.

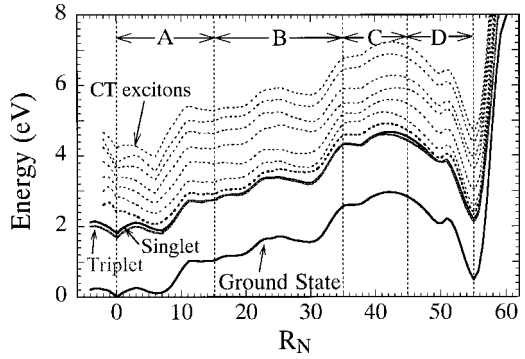

FIG. 10. The adiabatic potential energy curves of the ground state and the lowest singlet and triplet excitons relevant to the dimerization process. The point of $R_N=0$ corresponds to the Franck-Condon state and $R_N=55$ is the most stable dimerized structure in the crystal.

path in this stage is indicated by the thick arrow in this figure. For this region *D*, we assign $R_N=45-55$.

C. Adiabatic potential energy curves of Frenkel and CT excitons

Let us see the adiabatic potential energy curves of the ground state and the lowest singlet and triplet excitons relevant to the dimerization process. These potentials are depicted in Fig. 10 by the solid lines as a function of R_N. The point at $R_N=0$ corresponds to the Franck-Condon state, and $R_N=55$ is the most stable dimerized structure in the crystal, as defined before.

The overall feature of the adiabatic potential energy curves calculated here is quite characteristic in the following sense. The potential curves of the lowest singlet and triplet excitons change and become approximately parallel to that of the ground state through the structural changes from the fcc to the dimer. The energies of the fcc and the dimerized structures are almost equal, and the energy barrier between them is about 2.5 eV. Moreover, these curves are quite uneven with several energy minimum points in the vicinity of $R_N=7$, 14, 34, and so on. These energy minima are mainly due to the difference of the molecular orientations as mentioned in Fig. 7. Therefore, these metastable structures are expected to exist as the structural defects at low temperatures even in the single crystal. Incidentally, it should be noted that dimerization occurs only in the crystal phase. In other words, the dimer, of course, is not isolated, and lattice distortion of the crystal is induced around the dimer. Therefore, the calculated energies of dimer, which are slightly higher than those of the fcc crystal, are reasonable even though the van der Waals bond in the fcc crystal is replaced by the two covalent bonds in the resulting dimer.

In order to clarify the relaxation of the CT excitons, let us see the density of states for the singlet CT excitons ($\equiv\rho_{\mathrm{CT}}$), which is calculated as

$$\rho_{\mathrm{CT}}(E)=\sum_n \Delta\rho_n^{(1-2)}\delta(E_n-E), \tag{3.2}$$

where

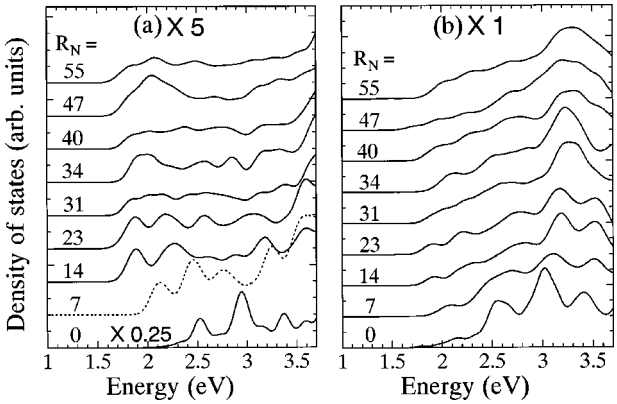

FIG. 11. The density of states for (a) the CT excitons ($\equiv\rho_{\mathrm{CT}}$) and (b) the non-CT excitons ($\equiv\rho_{\text{non-CT}}$) for various structures during the dimerization process.

$$\Delta\rho_n^{(1-2)}=\left|\sum_{i=1}^{60}\sum_{\sigma}\{\langle n|a_{1i\sigma}^{\dagger}a_{1i\sigma}|n\rangle-\langle n|a_{2i\sigma}^{\dagger}a_{2i\sigma}|n\rangle\}\right|,$$

$$0\leqslant\Delta\rho_n^{(1-2)}\leqslant 1. \tag{3.3}$$

$\Delta\rho_n^{(1-2)}$ is the absolute value of the total amount of the charge transfer between molecules 1 and 2 with respect to the nth one-electron singlet excited state with the energy E_n. We also calculate the density of states for the non-CT excitons ($\equiv\rho_{\text{non-CT}}$), defined as

$$\rho_{\text{non-CT}}(E)=\sum_n (1-\Delta\rho_n^{(1-2)})\,\delta(E_n-E). \tag{3.4}$$

Thus, $\rho_{\text{non-CT}}$ is regarded as the density of states for the Frenkel excitons. We show ρ_{CT} and $\rho_{\text{non-CT}}$ in Figs. 11(a) and 11(b), respectively. It can be seen from Fig. 11(a) that the peaks of ρ_{CT} shift toward the low-energy side as R_N increases from 0 to about 15. This is caused by the attractive interaction between the adjacent two molecules induced by the CT exciton. As shown in Fig. 11(b), on the other hand, $\rho_{\text{non-CT}}$ has no such clear shifts as ρ_{CT}, because the coupling between the Frenkel exciton and the intermolecular vibration is weaker than that of the CT exciton.

The peak energies of ρ_{CT}, which is regarded as the adiabatic potential energies of the CT exciton, are depicted by the dotted lines in Fig. 10. The expanded view in region *A* is also shown in Fig. 12. From Fig. 12, we can see that the potential surfaces of the CT exciton have a tendency to at-

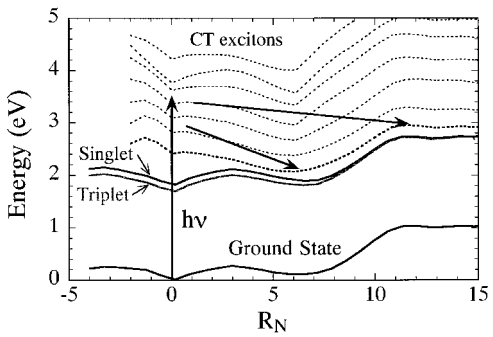

FIG. 12. The expanded view of the adiabatic potential energy curves in region *A* of Fig. 10.

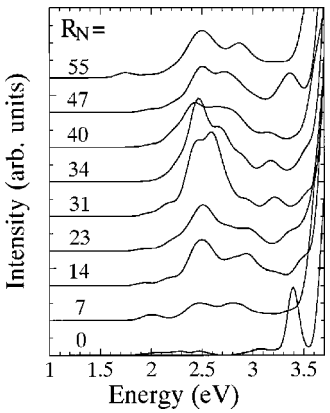

FIG. 13. The oscillator-strength distributions for various structures along the lattice relaxation path in the energy region below the fundamental absorption edge.

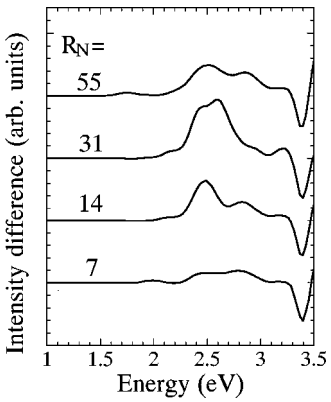

FIG. 14. The difference spectra of the oscillator strength distribution, which are calculated by subtracting the distribution in fcc from that in the metastable configurations appeared on the potential.

tract two adjacent molecules immediately after the photoexcitation, and the CT exciton will relax down to its self-trapped state, as appears at $R_N \approx 7$. Because the two molecules near each other as a result of self-trapping, it is concluded that the CT between two adjacent molecules is one of the trigger mechanisms for photoinduced dimerization. On the other hand, the adiabatic potential curve of the non-CT exciton, that is, the Frenkel exciton, is almost parallel to that of the ground state. These results imply that the lattice phonons couple strongly with the CT excitons rather than the Frenkel excitons. In this connection, Nakamura *et al.* have observed a time-resolved absorption spectrum in crystalline C_{60} by means of a femtosecond pump and probe spectroscopy. They have found that the exciton exhibits a two-component decay with a fast (1 ps) and a slow (>1 ns) decay times and have concluded that the fast decay component corresponds to the self-trapping of CT excitons.[20] Thus, the feature of the potential surfaces of the CT exciton near the Franck-Condon state gives qualitatively a good account for the experiments by the time-resolved spectroscopies.

IV. OSCILLATOR-STRENGTH DISTRIBUTIONS

Let us look at the oscillator-strength distributions thorough the lattice relaxation, so as to clarify the origins of the luminescence and the photoinduced absorption observed in crystalline C_{60}. In Fig. 13, we show the oscillator-strength distributions for various structures along the lattice-relaxation path in the energy region below the fundamental absorption edge. From this figure, we can see how the oscillator-strength distribution changes as the dimerization proceeds. In region A where R_N varies from 0 to 15, the distribution peak grows at about 2.5 eV. Because this peak has no energy shift, it is concluded that the origin of this peak is the Frenkel exciton, that is, the intramolecular electronic transition that is originally forbidden within the single molecule and then becomes optically allowed due to the increase of the intermolecular interaction as the two molecules approach. In this region, the other distribution peaks appear above 2.5 eV, and its energy shifts in concert with the changes in the density of states of CT excitons. Hence, the origin of these peaks is the CT exciton between two adjacent molecules. Moreover, near 1.9 eV we can see the weak peak that corresponds to the forbidden highest occupied molecular orbital–lowest unoccupied molecular orbital (HOMO-LUMO) transition of the single molecule. As the structural changes of the molecular cage proceed in regions C and D ($R_N = 35-55$), the distribution peaks around 2.5 eV shift toward both low- and high-energy sides, and the original lowest-energy peak at about 1.9 eV finally shifts down to about 1.7 eV in the final dimerized structure.

The excitation spectrum of the fluorescence has been observed for the C_{60} single crystal, and two types of the emission spectra have been found near 1.7 and 1.9 eV.[21,22] In fluorescence at low temperatures, photons are emitted mainly from the lowest electronic excited state that can optically couple to the ground state. Hence, the origins of these emissions are closely connected with the backward transition of the lowest-energy electronic excitation. Comparing these emission energies with the lowest-energy peaks of the calculated oscillator-strength distribution depicted in Fig. 13, we can conclude that the origin of the 1.9-eV emission is the fcc or structural defects, and that of the 1.7-eV emission is the dimerized structure.

Next, let us consider the origin of the photoinduced absorption spectra in crystalline C_{60}. These spectra have been observed by Bazhenov, Gorbunov, and Volkodav, and it has been found that the photoinjection of electron-hole pairs enhances the absorption at about 2.2 and 2.6 eV and broadly around 3 eV.[23]

In order to clarify the origins of these photoinduced peaks on the basis of the structural changes of the excitons predicted on the adiabatic potential energy curves obtained here, we calculate the difference spectra of the oscillator-strength distribution by subtracting the distribution in the fcc from that in the metastable configurations appearing on the potential. These difference spectra are shown in Fig. 14. From this figure, we can see that as the structural changes through the dimerization proceed, three peaks appear around the energies of 2.0, 2.5, and 2.8 eV, whose origins are the HOMO-LUMO transition, the Frenkel excitons, and the CT excitons, in order from low-energy side. These three peaks give fairly good agreement with the observed photoinduced absorption spectra. Therefore, it is concluded that the photoinduced spectrum is mainly given by the superposition of the absorption from the defects. This result means that the exciton created by the first photoexcitation relaxes down to its metastable

state, and the population of the structural defects increases in the ground state. As a result of this structural change, the absorption from the defects is enhanced in the second photoexcitation at the corresponding energy regions. Bazhenov, Gorbunov, and Volkodav have also observed thermal effects on the absorption spectra by raising the sample temperature by 4 K, and they have found that the intensity decreases in the energy region of 2.5 eV.[23] This spectral change is considered to come from the decrease of the population of the defects due to the heating.

Thus, the origin of the photoinduced absorption spectra are elucidated based on the photoinduced structural changes on the adiabatic potential energy surfaces obtained here. These results mean that the existence of the structural defects is indispensable for investigating the relaxation and/or the dynamics of excitons in crystalline C_{60} even in the single crystal.

V. DISCUSSION AND CONCLUSIONS

We have investigated the photoinduced-dimerization process in crystalline C_{60} using a model Hamiltonian, which is mainly based on the π-electron approximation together with the effective potential between carbons. The adiabatic potential energy surfaces of the CT and the Frenkel excitons relevant to photodimerization have been clarified by using the cluster model.

Let us briefly summarize the nature of the lattice relaxation of excitons in the crystalline C_{60} on the basis of the adiabatic potential energy surface obtained here. Just after the photogeneration of the exciton in the fcc single crystal of C_{60}, the free excitons are expected to induce a local lattice distortion. As this relaxation proceeds, we see the self-trapped exciton localized in the region of adjacent molecules, and then two molecules come close to each other through the CT-induced attractive interaction. From the analysis of the potential energy surfaces of the CT exciton, this self-trapped CT exciton is considered to be the precursor state of the dimerization process in the crystal. Therefore, the CT between two adjacent molecules is one of the trigger mechanisms for photodimerization or photopolymerization. On the other hand, the adiabatic potential curves of the Frenkel excitons are almost parallel to that of the ground state, and they are quite uneven with several energy minimum points. This leads to the conclusion that the various structural defects exist even in the single crystal at low temperatures as an intrinsic property in such molecular crystals, and they are indispensable for characterizing the photoinduced phenomena occurring in crystalline C_{60} as a prerequisite.

Finally, let us briefly speculate how dimerization is completed in crystalline C_{60}. The energy barrier between the fcc crystal and the dimer has been computed to be about 2.5 eV. So, it is difficult to proceed with dimerization through the relaxation of the relatively low-energy single exciton. Therefore, multiphotons are needed to achieve dimerization. Judging from the adiabatic potential energy curves, we can see that the exciton created by the first photon relaxes down mainly to the structural defect, namely, the intermediate state of the dimerization process. This intermediate state will have a long lifetime, so that it has a chance to be excited further by subsequent photons. This stepwise multiphotoexcitation will lead to the successive structural changes, and then dimerization will be completed when the energy of such metastable states exceeds the energy barrier. This is the picture of the structural phase transition due to the stepwise multiphotoexcitation. Incidentally, this successive process will be directly observed in crystalline C_{60} by vibrational spectroscopy, because the phonon structures of the C_{60} molecule are well confirmed.

ACKNOWLEDGMENTS

One of us (M.S) would like to thank Professor A. Nakamura and Professor K. Kan'no for providing us with valuable information.

[1] H. W. Kroto, J. R. Heath, S. C. O'Brien, R. F. Curl, and R. E. Smalley, Nature (London) **318**, 162 (1985).
[2] H. W. Kroto, J. E. Fischer, and D. E. Cox, *The Fullerenes* (Pergamon, Oxford, 1993).
[3] C. S. Yannoni, P. P. Bernier, D. S. Bethune, G. Meijer, and J. R. Salem, J. Am. Chem. Soc. **113**, 3190 (1991).
[4] P. A. Heinly, J. E. Fisher, A. R. McGhie, W. J. Romanow, A. M. Denenstein, J. P. McCauley, Jr., A. B. Smith, III, and D. E. Cox, Phys. Rev. Lett. **66**, 2911 (1991).
[5] W. I. F. David, R. M. Ibberson, J. C. Matthewman, K. Prassides, T. J. S. Dennis, J. P. Hare, H. W. Kroto, R. Taylor, and D. R. M. Walton, Nature (London) **353**, 147 (1991).
[6] A. M. Rao, P. Z. Zhou, K.-A. Wang, G. T. Hager, J. M. Holden, Y. Wang, W.-T. Lee, X. X. Bi, P. C. Eklund, D. S. Cornett, M. A. Duncan, and I. J. Amster, Science **259**, 955 (1993).
[7] I. O. Bashkin, A. N. Izotov, A. P. Moravsky, V. D. Negrii, R. K. Nikolaev, Y. A. Ossipyan, E. G. Ponyatovsky, and E. A. Steinman, Chem. Phys. Lett. **272**, 32 (1997).
[8] *Relaxations of Excited States and Photo-Induced Structural Phase Transitions*, edited by K. Nasu (Springer, Berlin, 1997).
[9] M. Suzuki and K. Nasu, Synth. Met. **64**, 247 (1994).
[10] M. Muccini, R. Danieli, R. Zamboni, C. Taliani, H. Mohn, W. Muller, and H. U. ter Meer, Chem. Phys. Lett. **245**, 107 (1995).
[11] J. Arbogast, A. Darmanya, C. Foote, Y. Rubin, F. Diederrich, M. Alvarez, S. Anz, and R. Whetten, J. Phys. Chem. **95**, 11 (1991).
[12] M. Terajima, N. Hirota, H. Shinohara, and Y. Saito, J. Phys. Chem. **95**, 9080 (1991).
[13] H. Ajie, M. M. Alvarez, S. J. Anz, R. D. Beck, F. Diederich, K. Fostiropoulos, D. R. Huffman, W. Kratschmer, Y. Rubin, K. E. Schiriver, D. Sensharma, and R. L. Whetten, J. Phys. Chem. **94**, 8630 (1990).
[14] J. H. Weavewr, J. L. Martins, T. Komeda, Y. Chen, T. R. Ohno, G. H. Kroll, N. Troullier, R. E. Haufler, and R. E. Smalley, Phys. Rev. Lett. **66**, 1741 (1991).
[15] F. Diederich and R. L. Whetten, Acc. Chem. Res. **25**, 119 (1992).
[16] M. K. Kelly, P. Etchegoin, D. Fuchs, W. Kratschmer, and K. Foostiropulos, Phys. Rev. B **46**, 4963 (1992).
[17] E. Sohmen, J. Fink, and W. Kratschmer, Z. Phys. B: Condens. Matter **86**, 87 (1992).

[18] V. Capozzi, G. Casamassima, G. F. Lorusso, A. Minafra, R. Piccolo, T. Trovato, and A. Valentini, Solid State Commun. **98**, 853 (1996).
[19] T. Tsubo and K. Nasu, Solid State Commun. **91**, 907 (1994).
[20] A. Nakamura, M. Ichida, T. Yajima, H. Shinohara, and Y. Saito, J. Lumin. **66&67**, 383 (1996).
[21] D. J. van der Heuvel, I. Y. Chan, E. J. J. Groenen, M. Matsushita, J. Schmidt, and G. Meijer, Chem. Phys. Lett. **233**, 284 (1995).
[22] I. Akimoto, J. Azuma, M. Ashida, and K. Kan'no, J. Lumin. **76&77**, 206 (1998).
[23] A. V. Bazhenov, A. V. Gorbunov, and K. Volkodav, Pis'ma Zh. Eksp. Teor. Fiz. **60**, 326 (1994) [JETP Lett. **60**, 331 (1994)].